Dynamics and Practical Predictability of Extratropical Wintertime Low-Frequency Variability in a Low-Dimensional System

MASARU INATSU AND NAOTO NAKANO

Graduate School of Science, Hokkaido University, Sapporo, Japan

HITOSHI MUKOUGAWA

Disaster Prevention Research Institute, Kyoto University, Uji, Kyoto, Japan

(Manuscript received 14 February 2012, in final form 28 August 2012)

ABSTRACT

Dynamics and practical predictability of extratropical low-frequency variability (LFV) in Northern Hemisphere winter are examined in the framework of a two-dimensional (2D) stochastic differential equation (SDE) on the phase space spanned by two leading empirical orthogonal function modes of low-pass-filtered 500-hPa geopotential height variations. The drift vector and diffusion tensor of the 2D SDE with multiplicative noise are theoretically connected with deterministic and stochastic error growth, respectively; both are statistically estimated from a reanalysis dataset. Projected onto the 2D phase space is the practical predictability of the LFV estimated by the 10-day forecast spread based on the 1-month ensemble prediction operationally conducted by the Japan Meteorological Agency (JMA). It is shown that the forecast spread of the LFV prediction by the JMA model for a relatively shorter prediction period when the model bias does not hamper the forecast is primarily explained by the stochastic error growth associated with the diffusion tensor and the deterministic error growth due to the Jacobian of the drift vector plays a secondary role. A non-Gaussian PDF of the LFV is also related to the norm of the diffusion tensor. Hence, the stochastic processes mostly control the dynamics and predictability of the LFV in the 2D phase space.

1. Introduction

The atmospheric low-frequency variability (LFV) with week-to-month time scales is characterized by disordered or chaotic nature but contains some ordered and persistent states, such as blocking and teleconnection patterns, which have been believed to be a key element of subseasonal prediction. Charney and DeVore (1979) regarded two stable fixed points as zonal and blocked weather regimes in their low-dimensional barotropic model with an idealized topography for the extratropical large-scale flow, and hypothesized that synoptic-scale fluctuations trigger a regime-to-regime transition. Some focused their attention on seeking fixed points in a nonlinear deterministic system so as to comprehensively explain the LFV's behavior. Quasi-stationary states are actually realized when a trajectory passes near fixed points (Legras and Ghil 1985) and local minimum points (Mukougawa 1988) in a phase space, and multiple equilibria associated with those points were found in several low-dimensional models (Cehelsky and Tung 1987; Itoh and Kimoto 1996; Reinhold and Pierrehumbert 1982). However, multiple equilibria can hardly be presented in more complex systems such as general circulation models (GCMs) with a huge number of variables. Efforts to find multiple weather regimes in the observed atmospheric motion have also been spurred (Kimoto and Ghil 1993; Mo and Ghil 1988; Molteni et al. 1990), with laboring over the search of multimodality in a low-dimensional phase space spanned by statistically obtained leading modes of LFV. Such difficulty in finding multiple weather regimes in the observation and complex models has been a stumbling block to apply a dynamic concept derived in a low-dimensional dynamic system to the real atmosphere. The difficulty comes from the implicit assumption that the high-dimensional atmospheric system can be reduced to a low-dimensional dynamic system by

Corresponding author address: Dr. Masaru Inatsu, Graduate School of Science, Hokkaido University, Rigaku Bldg. 8, N10W8, Kita, Sapporo 0600810, Japan.
E-mail: inaz@mail.sci.hokudai.ac.jp

DOI: 10.1175/JAS-D-12-048.1

neglecting nonlinear feedbacks through high-frequency variability and many aspects with limiting modes, variables, or domains.

The variation of the predictability of the LFV in the phase space has been also examined to seek a plausible dynamic relationship between predictability and atmospheric LFV. Kimoto et al. (1992) investigated a case that the subseasonal predictability got worse at the timing when the atmospheric state changed from zonal to blocking regimes. Palmer (1988) reported a better prediction in the positive phase of the Pacific–North American (PNA) pattern. Recently, Tang et al. (2007) suggested that the atmospheric large-scale motion is less (more) predictable in the negative (positive) phase of the Arctic Oscillation (AO). As for a low-dimensional system, Mukougawa et al. (1991) and Yamane and Yoden (1997) successfully captured a tendency that the atmospheric flow is more (less) predictable when it approaches (leaves) a quasi-stationary state or a weather regime. The above two studies only shed light on a particular relationship between predictability and quasi-stationary states, however. A decade has passed since we were standing at the difficulty of reducing a huge number of dimensions and of pursuing the general relationship between predictability and LFV. We are still far from fully understanding the predictability of the LFV all over the phase space in the framework of the deterministic nonlinear dynamic system.

On the other hand, the framework of a stochastic differential equation (SDE) has been recently used in the discussion of the atmospheric LFV (Berner 2005; Sura et al. 2005). The SDE in the Itô calculus (Hasselmann 1976; Penland and Matrosova 1998) is written as

$$dx_i = A_i(\mathbf{x})dt + \sum_j S_{ij}(\mathbf{x})dW_j, \tag{1}$$

where $\mathbf{x} = \mathbf{x}(t)$ is an atmospheric state vector, $\mathbf{A}(\mathbf{x})$ is called deterministic drift, $\mathbf{S}(\mathbf{x})$ is a state-dependent coefficient tensor for multiplicative noise, and $\mathbf{W}$ is the Wiener process vector, of which components are independent of each other. See Paul and Baschnagel (1999) for more detailed discussion on SDEs. The associate Fokker–Planck equation (FPE) that can be derived from Eq. (1) is written as

$$\frac{\partial P}{\partial t} = -\sum_i \frac{\partial}{\partial x_i} A_i(\mathbf{x})P + \sum_{i,j} \frac{\partial^2}{\partial x_i \partial x_j} B_{ij}(\mathbf{x})P, \tag{2}$$

where $P = P(\mathbf{x}, t)$ denotes the probability density function (PDF) of the state vector and the diffusion tensor $\mathbf{B} = (1/2)\mathbf{S}\mathbf{S}^{\mathrm{T}}$. Following Berner (2005) and Sura et al. (2005), the FPE coefficients of $\mathbf{A}$ and $\mathbf{B}$ are respectively approximated as

$$A_i \cong \left\langle \frac{\Delta x_i}{\Delta t} \right\rangle, \tag{3}$$

and

$$B_{ij} \cong \left\langle \frac{\Delta x_i \Delta x_j}{2\Delta t} \right\rangle, \tag{4}$$

where $\Delta x_i = x_i(t + \Delta t) - x_i(t)$, the angle brackets denote an ensemble average, and Δt is a short, finite time interval. Sura et al. (2005) indicated that a linear system with multiplicative noise could generate a climatological PDF that departed from the multivariate Gaussianity. In contrast, Branstator and Berner (2005) prudently insisted that a nonlinearity inherent in the planetary wave dynamics maintains multiple weather regimes in the LFV in a very long-term GCM simulation. Nonlinear deterministic versus linear stochastic approaches to LFV are still controversial, but we do not intend to get involved with this debate. Rather, we will pursue a new approach to explain the variation of the subseasonal predictability of the LFV in the framework of SDE or FPE. In fact, the fluctuation dissipation relation derived from the SDE [Eq. (1)],

$$\frac{d}{dt}\langle x_i x_j \rangle = \langle x_i A_j \rangle + \langle x_j A_i \rangle + 2\langle B_{ij} \rangle, \tag{5}$$

is quite suggestive of an intimate relationship between forecast spread and the atmospheric states. If the second moment of atmospheric states is stationary, the PDF is maintained with a macroscopic balance between the decay by deterministic dynamics [the first and second terms on the rhs of Eq. (5)] and the diffusion by stochastic processes [the last term on the rhs of Eq. (5); Penland 2003]. Recent promising climate modeling researches on tropical-to-extratropical atmospheric LFV (Newman et al. 2003), extratropical cyclone statistics (Whitaker and Sardeshmukh 1998), and tropical sea surface temperatures (SSTs; Penland and Matrosova 1998) actually used the fluctuation dissipation relation [Eq. (5)]. However, the linkage of the FPE coefficients with the subseasonal predictability has not been explored theoretically.

The purpose of this study is to develop a theory on the error growth based on the SDE and then to examine the relationship between the FPE coefficients and the subseasonal predictability in the 2D phase space spanned by the bases statistically obtained through the empirical orthogonal function (EOF) analysis for wintertime extratropical LFV data. The multiplicative noise in the SDE includes not only the nonlinear effect of high-frequency variability but also the effects of unresolved higher-order LFV components and the external forcing.

Hence, in projecting huge-dimensional motions into the 2D phase space, the deterministic drift vector as in Eq. (3) is probably statistically insignificant, whereas the stochastic noise statistics as in Eq. (4) are possibly significant. The newly constructed theory can estimate the deterministic and stochastic contribution to the error growth, so that we may reveal the relationship between forecast spread and FPE coefficients in a low-dimensional system.

This paper moreover compares the empirical error growth, or the FPE coefficients, based on a reanalysis dataset with the forecast error growth of the Japan Meteorological Agency (JMA)'s 1-month prediction model. Practically any model has a bias that is likely to deteriorate the predictability of the atmospheric motion. However, for a medium-range forecast of a prediction period shorter than 10 days where the model bias does not much affect the prediction, we can expect that the empirical error growth provides dynamic arguments to explain the characteristics of the practical predictability of the LFV based on the JMA's 1-month prediction model. Of course, for an extended-range forecast such as seasonal prediction where the model bias crucially affects the prediction, the above argument would lose its dynamic background.

At present, faster-speed supercomputers enables forecast centers such as the JMA, European Centre for Medium-Range Forecasting, and National Centers for Environmental Prediction to run a higher-resolution model with greater ensemble members. The forecast data that have been archived in the centers amount to as much as we manage to draw a projection map of forecast spread onto the 2D phase space, even though the data length is certainly shorter than that ideally required for a statistical significance. We note that this paper does rule out the work to prove that our newly developed theory on the empirical error growth in the 2D phase space exactly provides the forecast error growth in the perfect model. Instead, we invoke the new theory to explain the practical predictability of the LFV assessed by the ensemble spread of the JMA's 1-month prediction model. This attempt is based on the so-called perfect model assumption (Kalnay 2003) where the influence of the model bias should be minimized.

The rest of the paper is organized as follows: Section 2 describes forecast and reanalysis data and prepares the 2D phase space, section 3 explains the theoretical background to link the FPE coefficients with subseasonal predictability, section 4 shows subseasonal predictability and statistically estimated error growth based on the SDE projected onto the 2D phase space and illustrates the statistical stability of the FPE coefficients, and section 5 concludes the paper.

2. Data and method

We used the operational 1-month ensemble forecasts of the JMA in December–February (DJF) from 2001/02 to 2009/10. The JMA has conducted the forecast every Wednesday and Thursday using a global spectral model. The current forecasting system after March 2006 contains 25 ensemble members in each prediction using a model with TL155 (comparable to horizontal resolution of 110 km) and 40 vertical levels up to 0.1 hPa, while the previous prediction system before February 2006 used a T106L40 model with 13 ensemble members. The initial perturbation for the ensemble forecast was created by the breeding of growing modes method. This study used 500-hPa geopotential height in 216 ensemble forecasts.

The analysis data that we used are 6-hourly Japanese 25-yr Reanalysis/JMA Climate Data Assimilation System (JRA-25/JCDAS) dataset (Onogi et al. 2007). The grid interval is 1.25° in longitude by 1.25° in latitude, which is dense enough to analyze the global-scale LFV. The period is from 1979 to 2010, which is long enough to project the data onto a 2D phase space. Following many previous observational studies using a low-dimensional phase space, we used 500-hPa geopotential height that well represents significant characteristics of the LFV in the troposphere. The LFV were extracted by taking a low-pass filter of the 10-day running average throughout the period to exclude high-frequency eddies. An LFV anomaly is defined as the deviation from the LFV climatology. The analysis is limited in DJF.

We next defined a 2D phase space spanned by statistically obtained leading modes of the LFV anomaly north of 20°N in DJF from 1979/80 to 2009/10 (Fig. 1). We did not choose the phase space spanned by the leading modes obtained from a long-term integration of the forecast model because the 10-day forecast will be insignificantly influenced by the model bias (Mukougawa et al. 2009). As Quadrelli and Wallace (2004) and Itoh (2008) suggested, most teleconnection patterns are well represented by a linear combination of these two modes. For example, the AO (Thompson and Wallace 2000) is represented by a back-and-forth motion along a line connecting between the second and fourth quadrant of this 2D phase space. In fact, the AO index is highly correlated with an index linearly composed of the second principal component (PC) and the first PC with the reversed sign (correlation coefficient is about 0.8). The PNA pattern is almost parallel to the first EOF axis (Wallace and Gutzler 1981). Note that the obtained EOF modes are almost identical to those in Kimoto and Ghil (1993) including their sign. Because the first and second modes explain only 14.6% and 11.6% of the total

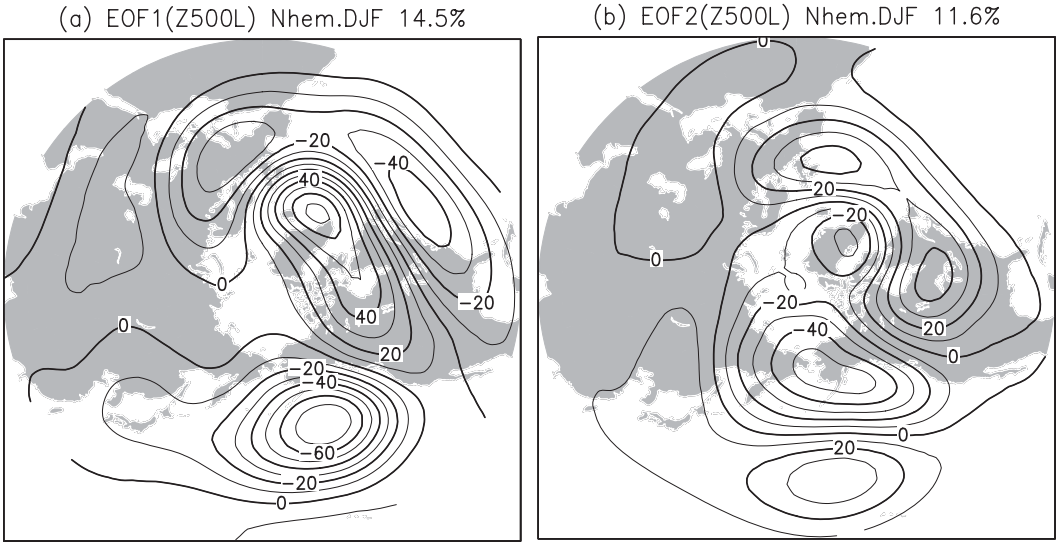

FIG. 1. (a) First and (b) second EOFs of 10-day low-pass-filtered geopotential height at 500 hPa in DJF from 1979/80 to 2009/10 based on 6-hourly JRA25/JCDAS dataset. Contour interval is 10 m with negative contours dashed.

variance of the LFV, respectively, we should care about the lack of information by boldly limiting a huge-dimensional motion to the 2D phase space in the analysis.

The DJF-mean Niño-3.4 index is used as an index of interannual variations of El Niño–Southern Oscillation (ENSO). DJF seasons with a positive (negative) Niño-3.4 index are classified as the warm (cold) phase of the ENSO in this paper.

3. Theory

a. Conventional theory

Before developing our new theory on the initial error growth by taking account of multiplicative noise, we begin with the conventional deterministic error growth theory (cf. Kalnay 2003). Any forecast model systems can be symbolically written as a nonlinear deterministic system of

$$\frac{d\mathbf{x}}{dt} = \mathbf{A}(\mathbf{x}). \tag{6}$$

The tangential linear equation around a particular state vector is derived from Eq. (6) as

$$\frac{dy_i}{dt} = \sum_j \frac{\partial A_i}{\partial x_j} y_j \equiv \sum_j J_{ij} y_j, \tag{7}$$

where $\mathbf{y} = \mathbf{y}(t)$ is the error vector and $\mathbf{J}$ is the Jacobian matrix of $\mathbf{A}$. Formally solving Eq. (7) with an initial error vector at $t = 0$, $\mathbf{y}(0)$, then

$$y_i(t) = \sum_j M_{ij}(t,0) y_j(0), \tag{8}$$

where $\mathbf{M}(t, 0)$ denotes the error matrix (Lorenz 1965). The singular value decomposition (SVD) analysis for the error matrix is

$$\mathbf{M}(t,0)\mathbf{v}^{(m)} = \sigma_D^{(m)}\mathbf{u}^{(m)}, \tag{9}$$

providing two sets of orthonormal bases of $\mathbf{v}^{(m)}$ and $\mathbf{u}^{(m)}$, which are the mth mode of the initial and final error vector, respectively. The spread of the initial error for the error matrix is derived from Eq. (8) as $\widetilde{E_D} = \varepsilon\sigma_D^{(1)}$, where ε denotes the magnitude of the initial perturbation.

b. New theory

We now develop a theory for the error growth with the SDE as already introduced in Eq. (1). The SDE is rewritten in the integral form as

$$x_i(t) = x_i(0) + \int_0^t A_i(\mathbf{x})\, d\tau + \int_0^t \sum_j S_{ij}(\mathbf{x})\, dW_j. \tag{10}$$

Taking an ensemble mean for Eq. (10), then

$$\langle x_i(t)\rangle = \langle x_i(0)\rangle + \int_0^t \langle A_i(\mathbf{x})\rangle\, d\tau. \tag{11}$$

Subtracting Eq. (11) from Eq. (10), the deviation from the ensemble-mean state follows

$$\delta x_i(t) - \delta x_i(0) = \int_0^t \delta A_i(\mathbf{x})\, d\tau + \int_0^t \sum_j S_{ij}(\mathbf{x})\, dW_j, \tag{12}$$

where $\delta x_i = x_i - \langle x_i \rangle$ and $\delta A_i = A_i - \langle A_i \rangle$. Provided that ergodicity permits us to replace the ensemble mean with the intermittent temporal average over a finite subdomain in the phase space, the deterministic drift can be estimated as the ensemble mean of the time evolution of the atmospheric state vector in the phase space as Eq. (3). We hereafter assume that the Jacobian matrix of **A** is independent of the stochastic processes in a tangential linear system.

First the temporal evolution of the error growth by deterministic processes follows

$$\delta x_i(t) = \sum_j M_{ij}(t,0)\delta x_j(0), \tag{13}$$

just like the conventional error growth theory. The spread for the deterministic error matrix is therefore derived from Eq. (13) as

$$E_D = \varepsilon \|\mathbf{M}(t,0)\|. \tag{14}$$

Remark that the error matrix with relatively short forecasting period can be approximated by

$$\mathbf{M} \cong \exp(t\mathbf{J}) \cong \mathbf{I} + t\mathbf{J}, \tag{15}$$

where the norm of **J** is derived from the spatial difference of **A**.

Next, using an analogy in the derivation of the fluctuation dissipation relation [Eq. (5)] from Eq. (12), the equation of the error covariance matrix is obtained as

$$\langle \delta x_i(t)\delta x_j(t)\rangle - \langle \delta x_i(0)\delta x_j(0)\rangle = \int_0^t \langle \delta x_i \delta A_j\rangle \, d\tau + \int_0^t \langle \delta x_j \delta A_i\rangle \, d\tau + \int_0^t 2\langle B_{ij}\rangle \, d\tau. \tag{16}$$

The first and second terms in the rhs are related to the Jacobian matrix:

$$\langle \delta x_i \delta A_j\rangle + \langle \delta x_j \delta A_i\rangle \cong \sum_k (J_{ik}\langle \delta x_j \delta x_k\rangle + J_{jk}\langle \delta x_i \delta x_k\rangle), \tag{17}$$

noticing that $\langle \mathbf{A}(\mathbf{x})\rangle = \mathbf{A}(\langle \mathbf{x}\rangle) + (1/2)\mathbf{A}''(\langle \mathbf{x}\rangle)\langle(\mathbf{x} - \langle \mathbf{x}\rangle)^2\rangle + \cdots \cong \mathbf{A}(\langle \mathbf{x}\rangle)$ and $\delta A_i = A_i(\mathbf{x}) - \langle A_i(\mathbf{x})\rangle \cong \sum_j \delta x_j J_{ij}(\langle \mathbf{x}\rangle)$. The same form can be easily derived from Eq. (8), if the error originated from the initial perturbation y_i is replaced with the deviation from the ensemble average δx_i. In a purely stochastic system, where the first two terms are ignored, the eigenvalue analysis for the diffusion tensor is

$$\mathbf{B}\mathbf{e}_S^{(m)} = \sigma_S^{(m)}\mathbf{e}_S^{(m)}, \tag{18}$$

providing a set of orthonormal bases of $\mathbf{e}_S^{(m)}$, and the time evolution of the ensemble spread for the stochastic processes is estimated by

$$E_S = (\varepsilon^2 + 2\|\mathbf{B}\|t)^{1/2} = (\varepsilon^2 + 2\sigma_S^{(1)}t)^{1/2}, \tag{19}$$

with the initial error with its variance ε^2. Note that all the eigenvalues are positive because the **B** is a positive Hermitian matrix. Following the previous studies (Berner 2005; Sura et al. 2005), **A** is statistically estimated by Eq. (3) and the diffusion tensor is also statistically obtained by Eq. (4), remarking that Δt in Eqs. (3) and (4) is set to 6 h in the analysis. Equations (14) and (19) therefore provide the way to evaluate the deterministic and stochastic error growth from an initial perturbation, respectively.

4. Results

a. Forecast spread

Figure 2 shows some forecast statistics of the operational 1-month ensemble prediction of the JMA in DJF from 2001/02 to 2009/10. The statistics for the 10-day forecast projected onto the 2D phase space (section 2) were obtained based on the 10-day running average of 500-hPa geopotential height prediction north of 20°N, and they were plotted at each locus in the phase space for the initial date of the forecast. Following Sura et al. (2005), the plots are smoothed over 3×3 bins, each of which occupies a 0.4×0.4 tile squarely divided in the phase space. A total of 216 forecasts are scattered over there, and then a single bin contains a few forecasts even around the origin (Fig. 2a). The resultant projection therefore gives us only a very rough picture without bearing a usual statistical significance test in a bin-to-bin comparison, but the phase space distribution of the forecast spread is apparently nonuniform. The spread along the most- and least-growing directions on the phase space (Figs. 2c,d) as well as the total spread of 500-hPa geopotential height north of 20°N (Fig. 2b) show enhanced (reduced) predictability in the second (fourth) quadrant. The difference of the magnitude between these two subdomains is less than 10% for the total spread (Fig. 2b), but exceeds 20% for the spread along the most-growing direction (Fig. 2c) with a statistical significance at the 95% level.

Two points should be discussed regarding the statistics of the forecast spread. First, the error growth along the most-growing direction is moderately larger than that along the least-growing direction in the second quadrant (Figs. 2c,d). Figure 3 shows a scatterplot of the most-growing vector for ensemble forecasts of which initial

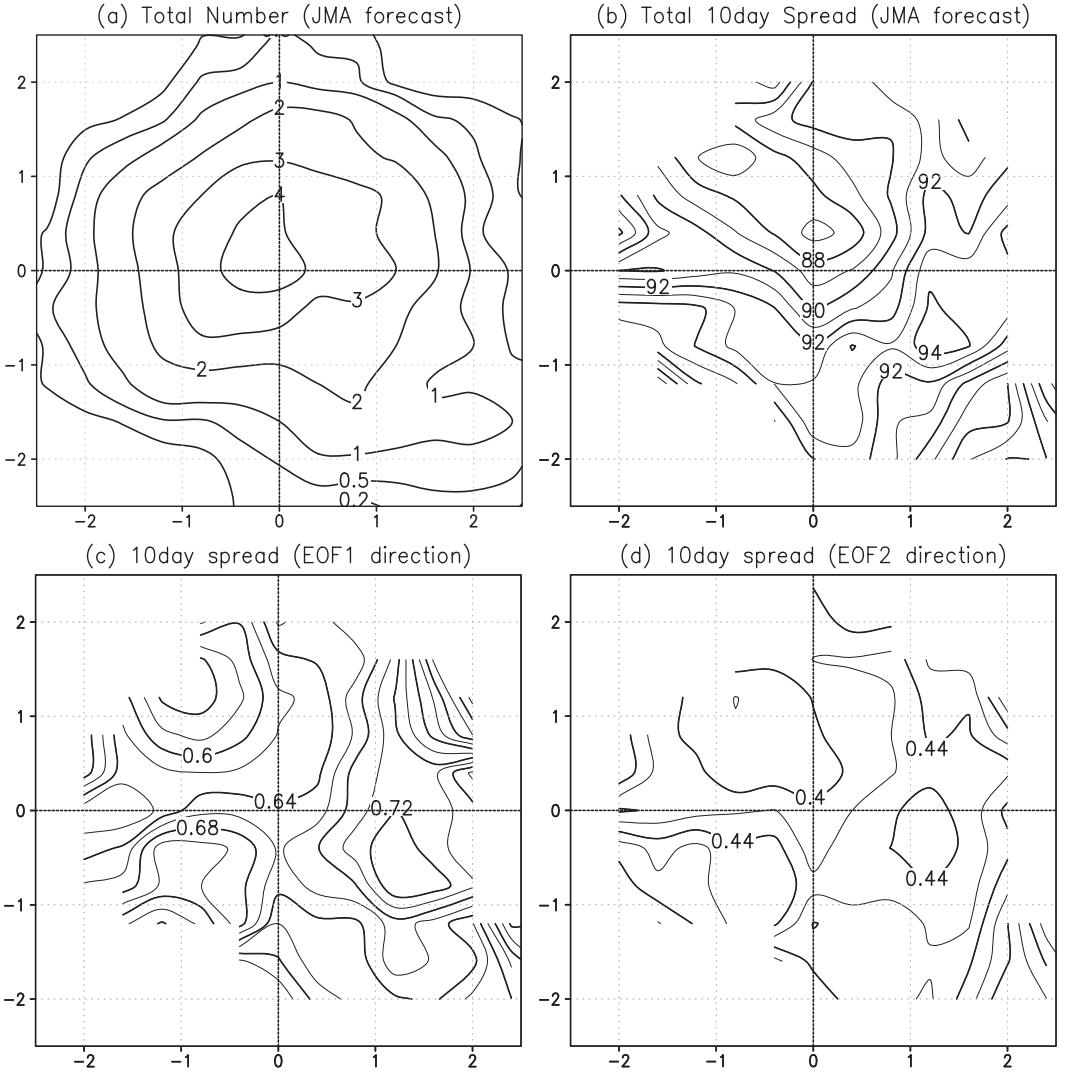

FIG. 2. Subseasonal predictability statistics smoothed over 3 × 3 bins on the phase space spanned by the two leading EOFs; each bin occupies a 0.4 × 0.4 tile. (a) The number of the JMA's forecasts in each bin with contours of 0.2, 0.5, 1, 2, 3, and 4. The area with the sampling number less than 0.5 is blanked out in other panels. (b) Forecast spread of 500-hPa geopotential height anomaly. Contour interval is 1 m. Spread at 10 forecast days along the (c) most- and (d) least-growing directions in the phase space. Contour interval is 0.02.

condition resides in each quadrant in the phase space. Note that a line segment connecting between each plotted point and origin denotes the magnitude and direction of each dimensional eigenvector. The majority of vector directs toward the second EOF axis with a small EOF1 component especially in the first, third, and fourth quadrant (Figs. 3a,c,d), where the most-growing vector has much larger magnitude than the least one (Figs. 2c,d). By contrast, there is no preferable direction for the most-growing vector in the second quadrant (Fig. 3b). Second, we have to check an influence of the forecast system renewal in 2006 (section 2). Figure 3 plots the most-growing vector with open circles for the previous system and with solid circles for the renewed one. We cannot find any significant difference between them, so we need not care about the system renewal effect in this study.

Our newly developed theory on the error growth (section 3) can deal with the stochastic growth represented by the diffusion tensor as well as the deterministic growth described by the Jacobian matrix. Note that the initial error variance is now set to 0.12, which roughly corresponds to the magnitude of the initial error of JMA operational 1-month ensemble forecast (not shown). The estimated spread E_D due to the Jacobian matrix [Eq. (14)] has a different distribution (Fig. 4a) from the projected spread on the most-growing direction for the

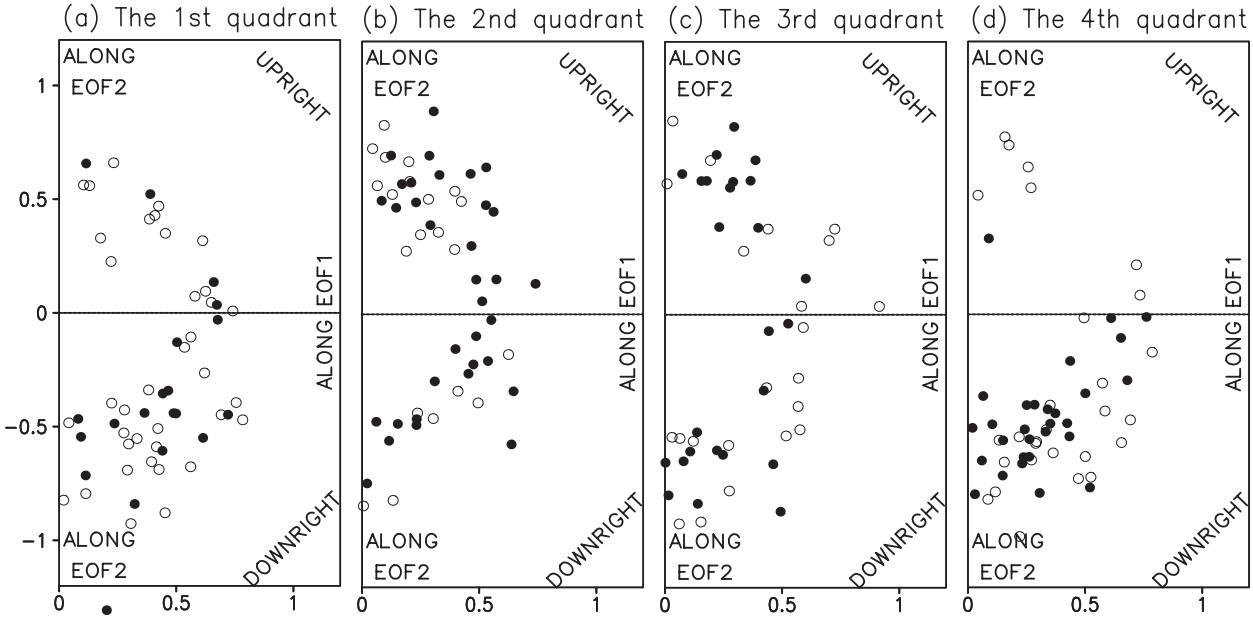

FIG. 3. Scatterplots of the direction of the most-growing mode for 10-day forecast spread in the (a) first, (b) second, (c) third, and (d) fourth quadrant. Open (solid) circles are plotted at the arrowhead of the most-growing vector from the origin for the forecasts before DJF 2005/06 (after DJF 2006/07). A line segment between plotted point and origin denotes the magnitude and direction of a dimensional eigenvector.

operational 10-day forecast of the JMA (Fig. 2c). It is slightly large in the fourth quadrant, but it seems rather uniform near the origin. Areas with large E_D reside far from the origin of the phase space, although the sample size is highly limited there. The estimated spread anywhere in the phase space is much smaller than the forecast spread $E \sim 0.65$ of the operational ensemble prediction for LFV (Fig. 2c). Moreover, the largest singular vector direction (tick marks in Fig. 4a) in the third and fourth quadrant is not always along the EOF2 axis, which is quite different from the most-growing direction of the operational forecast (Figs. 3c,d). On the other hand, the distribution of the estimated spread E_S (Fig. 4b) due to the stochastic processes [Eq. (19)] agrees well with that of the forecast spread (Fig. 2c) in the 2D phase space. Note that because the diffusion tensor term [$\int_0^t \langle B_{ij} \rangle \, d\tau$ in Eq. (16)] largely contributes to the error covariance matrix of $\langle \delta x_i \delta x_j \rangle$ in Eq. (16) shown in Fig. 4c, the first and second terms are indeed negligible in Eq. (16). The local maxima of the norm of the diffusion tensor are found in the third and fourth quadrant, while the local minima are located in the first to second quadrant and near (0, −2) in the phase space (Fig. 4b). The exception is a part of the first quadrant, where the ensemble spread (Fig. 2c) is rather large but the norm of the diffusion tensor is smallest in the phase space. The magnitude of the forecast error growth (Fig. 4b) due to the stochastic processes is about one-third smaller than the magnitude of the ensemble spread, perhaps because the JMA forecast model bias moderately expands the error growth. Thus, it is suggested that the forecast spread of 10-day ensemble prediction of the LFV in the 2D phase space is attributed to the stochastic processes. Furthermore, the first eigenvector of the diffusion tensor (tick marks in Fig. 4b) is parallel to the second EOF mode, similar to the most-growing direction of the forecast spread (Fig. 3). The estimated spread to the second eigenvector of the diffusion tensor, with the given initial error being 0.12 again (Fig. 4d), also agrees with the pattern of the ensemble forecast spread projected onto the least-growing direction (Fig. 2d).

Figure 5 shows the time evolution of the observed forecast spread (solid line) and the estimated initial error growth due to the deterministic process (dotted line) and that due to the stochastic processes (dashed line) against the forecast period for a particular initial location at (−1.2, −1.2) in the phase space. The magnitude of the initial error is set to 0.12 for these estimations as in Fig. 4. The observed forecast spread increases until its saturation period of about 3 weeks. The estimated spread due to the stochastic diffusion mostly follows it until 5 days and then increases more slowly than the operational forecast spread. On the other hand, the estimated error for the deterministic process is too slowly increasing, and its magnitude is much smaller than the observed forecast spread even within a short forecast period of a couple of days, in which the tangential linear equation is thought to precisely describe the initial error

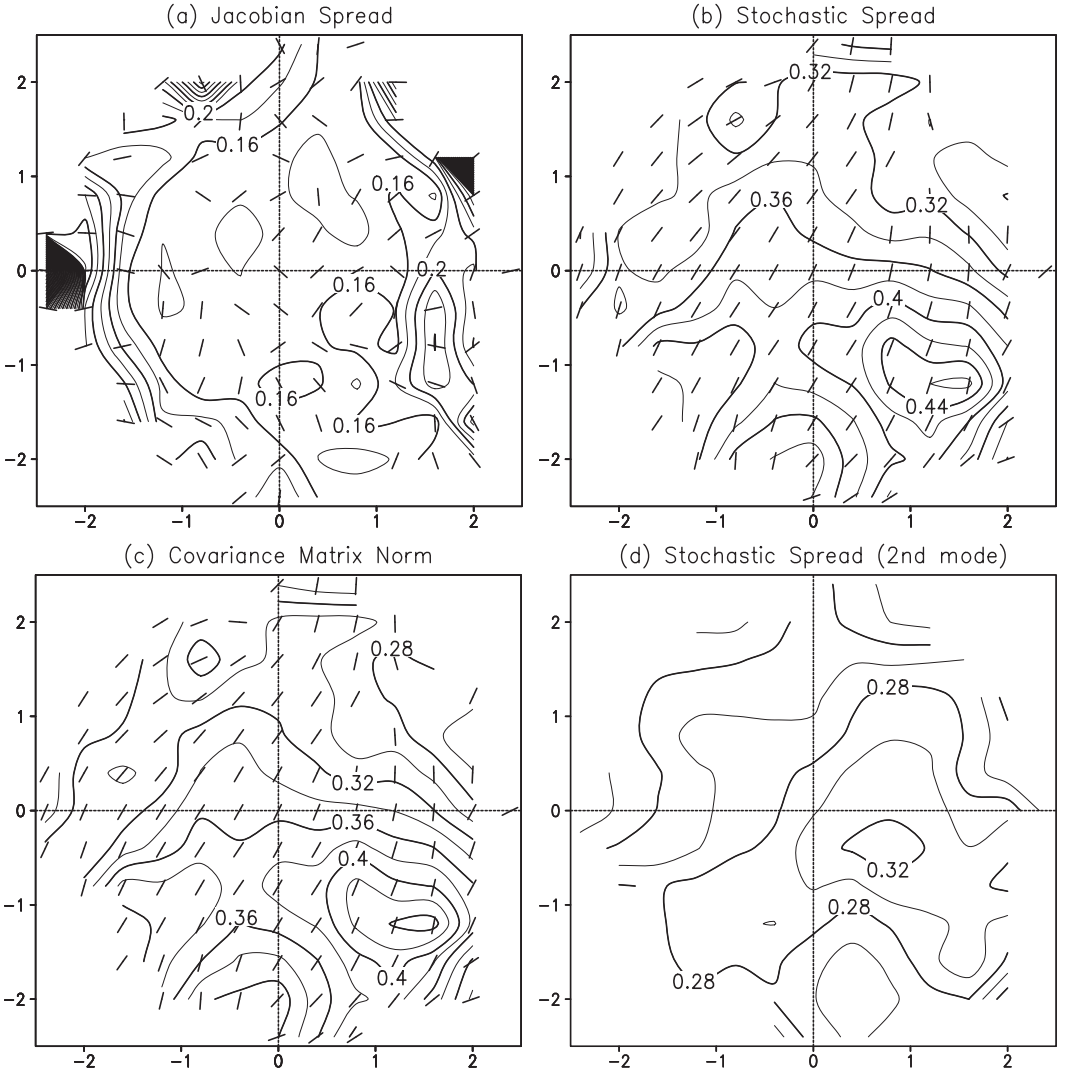

FIG. 4. The 10-day forecast spread due to the (a) deterministic Jacobian matrix and (b) stochastic diffusion tensor with the initial error variance fixed at 0.12. Contour interval is 0.02 (10 day)$^{-1}$. (c) The norm of the covariance matrix in Eq. (16). (d) The spread due to the second eigenvalue of diffusion tensor with the initial error variance fixed at 0.12 again. Tick marks in (a)–(c) denote the direction of the largest eigenvector of the error matrix, the diffusion tensor, and the covariance matrix, respectively.

growth. This supports the notion that the practical predictability of the extratropical LFV projected on a low-dimensional phase space can be assessed using the equation with the stochastic processes. The assessment is worthwhile for medium-range forecasts with near a 10-day period when the model bias insignificantly affects the prediction.

The climatological PDF distribution (Fig. 6) of the extratropical LFV by scattering 11 192 reanalysis data points[1] over the 2D phase space moreover indicates a link between the spread and the norm of the diffusion tensor. The non-Gaussian PDF distribution possibly suggests the existence of multiple weather regimes (Kimoto and Ghil 1993; Sura et al. 2005). In fact, the observed PDF is smaller than the bivariate Gaussianity in regions of the fourth quadrant far from the origin, while larger PDF than the Gaussianity is found in the first and the second quadrant. Areas with larger PDF than the Gaussianity are also located on the negative side of each axis. Interestingly, the overall distribution of the observed PDF is closely related to the distribution of the observed spread (Fig. 2c) and the estimated spread for stochastic

[1] Degrees of freedom are about 300 in the analysis period, because a low-pass filter was taken for the data.

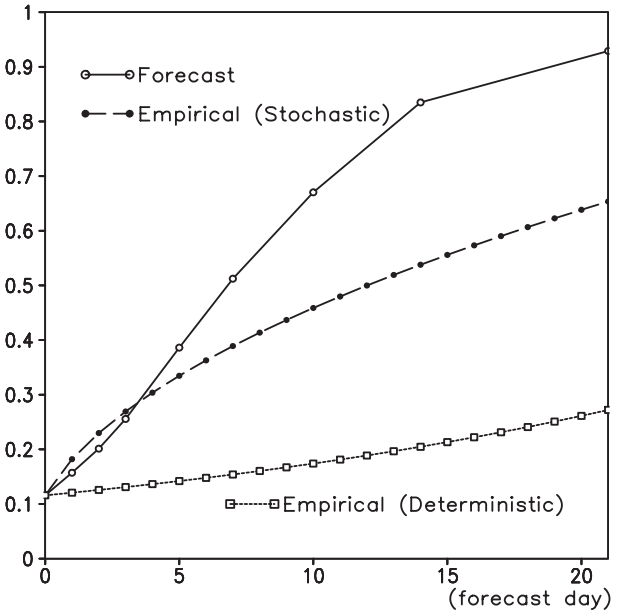

FIG. 5. Growth of ensemble forecast spread (solid), and empirically estimated spread for the stochastic diffusion (dashed) and the deterministic system (dotted) at (1.2, −1.2) in the phase space against the forecast period.

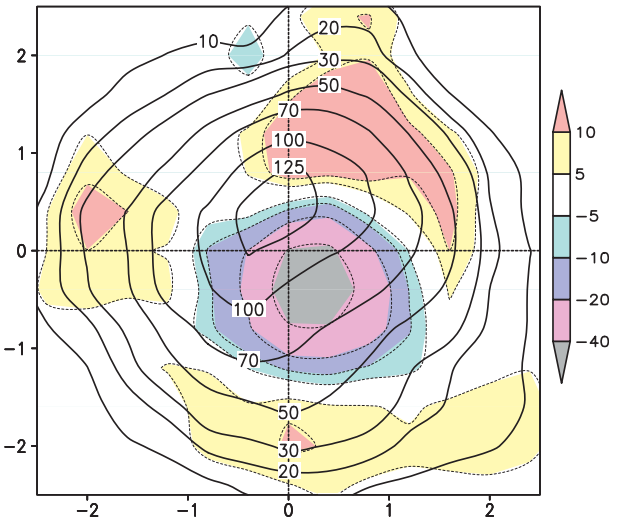

FIG. 6. The PDF of the two leading principal components (contour) and its departure from the bivariate Gaussianity (shading) (unit is 10^{-3}). Contours are drawn for 10, 20, 30, 50, 70, 100, and 125 $\times$ 10^{-3} and color shading is shown by the scale. The area with less than 0.01 PDF is blanked out in Figs. 4, 7, and 8.

processes (Fig. 4b). Three preferred regions along a circle whose center is at the origin and radius is about 1.5 in the 2D phase space (Fig. 6) coincide well with the loci with small norm of the diffusion tensor, while the fourth quadrant characterized by less frequency has a large norm of the diffusion tensor. Thus, the regions with the PDF larger than Gaussianity (i.e., weather regimes) could be formed through the smaller stochastic spread of the trajectory there.

b. *Statistical stability*

This subsection examines statistical stability of the FPE coefficients in terms of the relationship among them. Remembering $A_i \cong \langle \Delta x_i/\Delta t \rangle$ [Eq. (3)] and $B_{ij} \cong \langle \Delta x_i \Delta x_j/2\Delta t \rangle$ [Eq. (4)], we find the relation of

$$\left\langle \sum_i \left(\frac{\Delta x_i}{\Delta t} \right)^2 \right\rangle = \mathrm{trace}\left(\frac{2\mathbf{B}}{\Delta t} \right), \tag{20}$$

which means that the ensemble mean of the (squared) magnitude of the time evolution of state vector is proportional to the sum of all of the eigenvalues of **B**. As the first eigenvalue is much larger than the other(s), the norm of diffusion tensor is almost explained by the variance of time evolution of state vector. Figures 7a,b display the ensemble mean of the norm of $\Delta\mathbf{x}/\Delta t$ (i.e., $\langle \|\Delta\mathbf{x}/\Delta t\| \rangle$) and the norm of the ensemble-mean $\Delta\mathbf{x}/\Delta t$ (i.e., $\|\langle \Delta\mathbf{x}/\Delta t \rangle\|$), respectively. The former distribution is similar to the plot of the lhs of Eq. (20) (not shown), and the latter is the magnitude of drift vector in short. The magnitude of $\langle \|\Delta\mathbf{x}/\Delta t\| \rangle$ is much larger than that of $\|\langle \Delta\mathbf{x}/\Delta t \rangle\|$ even in the region far from the origin of the phase space. This means that any features of the drift vector shown in the vector plot of Fig. 7b are therefore statistically insignificant in the 2D phase space. The square root of the diffusion tensor norm (Fig. 7c) has a quite similar distribution to $\langle \|\Delta\mathbf{x}/\Delta t\| \rangle$, which is consistent with Eq. (20). Note that, since the trace of **B** is slightly larger than norm of **B** that is a positive Hermitian matrix, the plot of Fig. 7c is a bit smaller than that of Fig. 7a. Thus, this kind of highly truncated systems with reducing the dimension too much from the real atmospheric system must scatter the trajectory associated with the estimated diffusion tensor.

We further examine the statistical stability of the FPE coefficients from a different viewpoint. Traditionally, the ENSO is an effective agent of the external forcing to the PNA pattern (Geisler et al. 1985; Horel and Wallace 1981). In fact, Palmer (1999) illustrated an important role of the external forcing that potentially shifts the PDF of the extratropical LFV to a particular direction in the phase space. The composited drift vector for the warm and cold phases of the ENSO (Figs. 8a,b) suggests the importance of the external forcing (see section 2 for how the PC time series are divided into the warm and cold phases of ENSO). The drift vector is statistically unstable even with a larger magnitude than its average (Fig. 7b). The diffusion tensor norm, in contrast, holds the characteristics of its average distribution with the

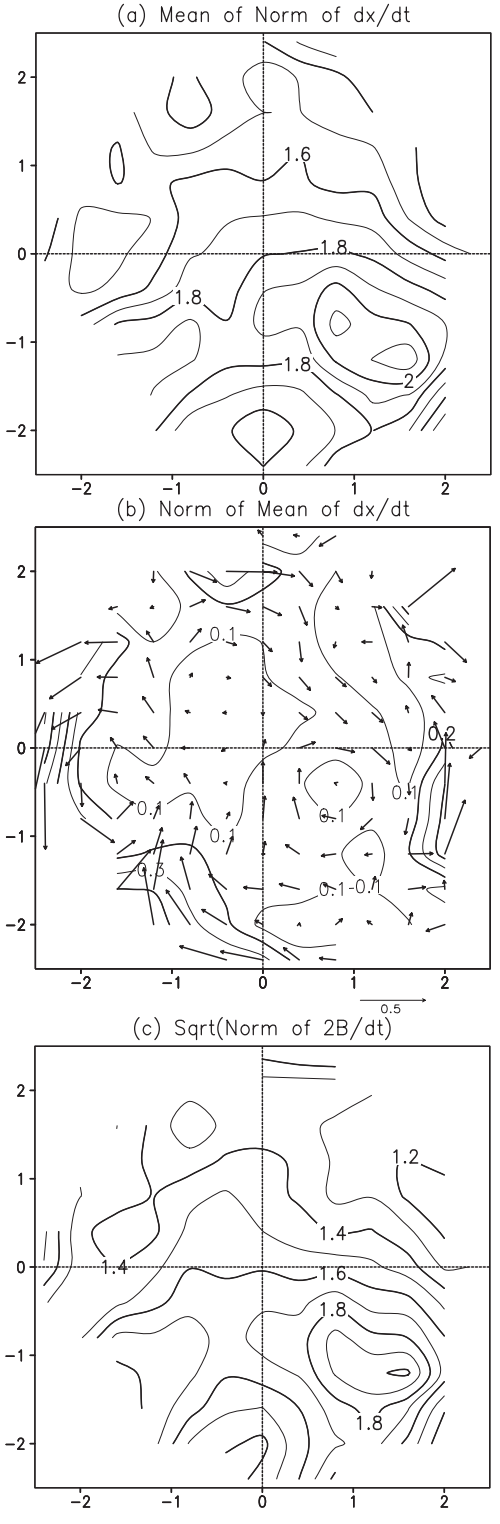

FIG. 7. (a) The ensemble mean of the norm of the time derivative of the atmospheric state vector. Contour interval is 0.1 $(10\ \text{day})^{-1}$ and the area with less than 0.01 PDF is blanked out. (b) The norm of **A** superimposed with the drift vector itself; the reference vector with its magnitude of 0.5 $(10\ \text{day})^{-1}$ is at the bottom right. (c) The square root of norm of $2\mathbf{B}\Delta t$.

local maximum in the fourth quadrant and smaller values in the upper half plane. Interestingly the drift vector shows an opposite direction in the fourth quadrant between two phases. This clear difference gives rise to the larger norm of the diffusion tensor in the total-period statistics there, so that the ENSO is thought of as a strong external forcing in this 2D system that, to some extent, brings statistical instability of the drift vector.

We next perform another division of the PC time series. The observed forecast spread (Fig. 2) is based on the operational 1-month forecast in 2001/02–2009/10 from the initial condition of the analysis data, which is also used in the estimation of the spread due to the deterministic and stochastic processes. To examine the effect of this duplicate use of the analysis data to the results, the data are split into 1990s and 2000s (Figs. 8c,d). The former period is completely independent to the operational forecast used in this paper. The difference of the diffusion tensor norm between these two periods is not so large. Hence, the diffusion tensor norm is so statistically stable that we need not care about the problem of the duplicate use of the analysis data after 2001/02.

5. Concluding remarks

This study investigated predictability and the dynamics of the extratropical LFV in terms of an SDE equation in the phase space constructed by the two leading modes for the LFV based on JRA-25/JCDAS data in DJF from 1979/80 to 2009/10. The ensemble spread of the operational 1-month prediction of the JMA in DJF from 2001/02 to 2009/10 was used to evaluate the practical predictability of the LFV. The 10-day forecast spread of 10-day running-mean 500-hPa geopotential height showed a nonuniform distribution of predictability in the 2D phase space, even though the data period of the ensemble prediction utilized in this study was too short to assure statistical significance. The distribution of the forecast spread and the norm of the diffusion tensor in the SDE in the 2D phase space were very similar to each other, but the norm of the Jacobian matrix obtained from the drift vector of the SDE has a totally different magnitude and distribution in the phase space. We thus suggest that the stochastic multiplicative noise expressed by the diffusion tensor can play a primary role in the forecast error growth in this low-dimensional phase space and show that the new theory can explain the characteristics of the practical predictability of the LFV assessed by the JMA's 1-month prediction model for a medium-range forecast where the model bias only insignificantly affects the forecast.

The predictability of the LFV was enhanced (reduced) in the second (fourth) quadrant of the 2D phase space

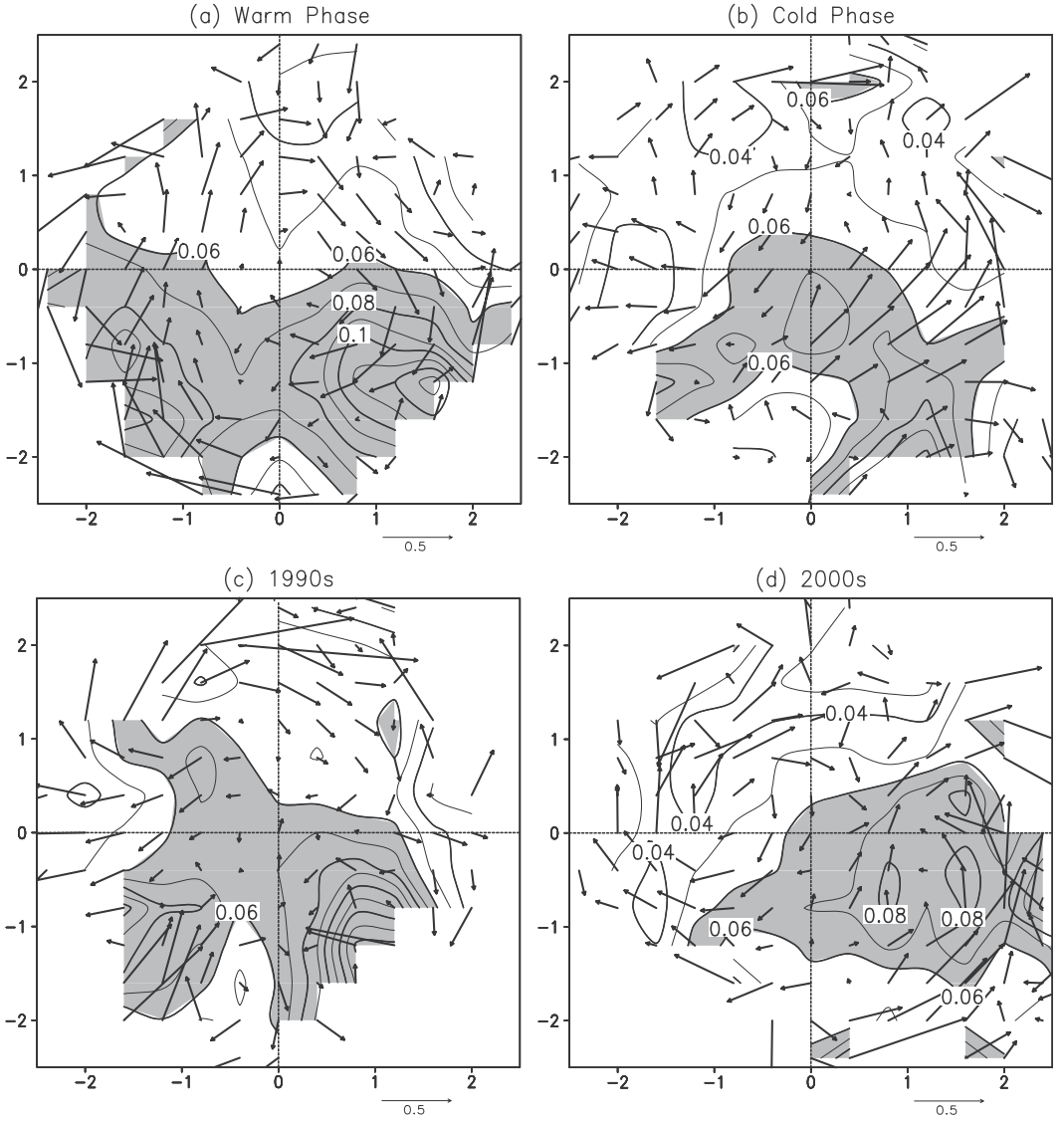

FIG. 8. The ensemble-mean drift vector (arrows) and diffusion tensor norm (contours) for the (a) warm and (b) cold phases of El Niño–Southern Oscillation. Contour interval is 0.01 (10 day)$^{-1}$, and the arrow size follows the reference in the bottom [unit is (10 day)$^{-1}$]. The area with diffusion tensor norm greater than 0.06 (10 day)$^{-1}$ is shaded. (c),(d) As in (a), but for the statistics in 1990/91–1999/2000 and 2000/01–2009/10, respectively.

(section 4). Figures 9a,b show the corresponding composite of zonal-mean zonal wind and the Eliassen–Palm flux for the second and fourth quadrant. The second-quadrant composite shows a wider and relatively weaker subtropical jet stream with active Rossby waves, while the fourth-quadrant composite shows a narrower and stronger subtropical jet with inactive Rossby waves. The difference of the composite maps, being statistically significant (Fig. 9c), resembles the regression map on the AO index (Fig. 9d). This is consistent with Tang et al. (2007), who suggested that the atmospheric large-scale motion is less (more) predictable in the negative (positive) phase of AO.

As documented in the introduction, the practical predictability examined in this paper inevitably depends on which forecast models one chooses. However, the practical predictability of the LFV assessed by a 10-day forecast spread of the JMA's 1-month prediction model has a qualitatively similar distribution in the 2D phase space to the empirically estimated predictability based on the SDE equation. The similarity implies that the 10-day forecast of the JMA model is reliable enough to represent the evolution of the LFV in the real atmosphere and is not much influenced by the model bias. On the other hand, for other LFV phenomena such as the Madden–Julian oscillation of which model prediction

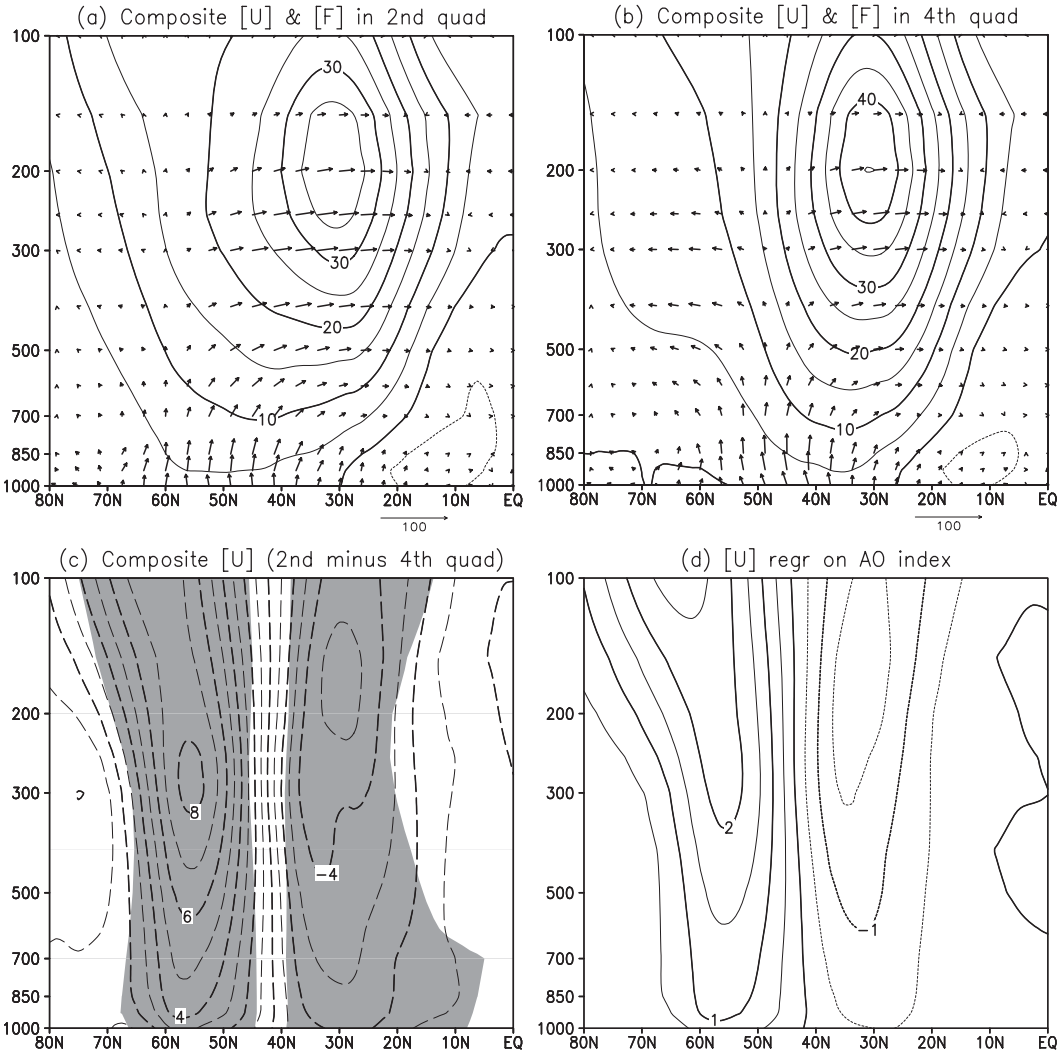

FIG. 9. Composite map of zonal-mean wind (contours) and the Eliassen–Palm flux (arrows) for the (a) second and (b) fourth quadrants. Contour interval is 5 m s^{-1}. The reference at the bottom denotes 100 kg m^{-1} s^{-2} horizontal component and 1 kg m^{-1} s^{-2} vertical component of the Eliassen–Palm flux. (c) The difference of the composited zonal-mean zonal wind between the second and the fourth quadrants (i.e., Fig. 9a − Fig. 9b). The contour interval is 1 m s^{-1} and the shading denotes the statistical significance at 95% level. (d) The regression of zonal-mean zonal wind on the Arctic Oscillation index with the contour interval of 0.5 m s^{-1}.

suffers from a significant model bias, the error growth of the forecast model would be much larger than the empirical error growth estimated by a long-term reanalysis dataset, and the temporal evolution of the error growth would be quite different between them (cf. Chikamoto et al. 2007). In such a case, the argument based on the SDE equation might be inadequate to examine the practical predictability.

One might imagine that an empirical SDE has a potential to propose a brand-new subseasonal forecast with a less computational cost. Unfortunately, an SDE forecast in the 2D phase space would not be so promising because the ensemble-mean drift vector is again much smaller than the observed time evolution of the trajectory (Figs. 7a,b). This issue could be relieved if we utilized the phase space with much higher dimension. We guess that the data length of about $10^{d/2}$ of DJF seasons is required to estimate the d-dimensional PDF.[2] The reanalysis data have been archived for about 30 yr,

[2] The degrees of freedom of data in a single DJF season are about 9. If you statistically calculated the one-dimensional PDF in a phase space, you would require about 30 independent samples. The required number of winters can then be roughly estimated by $10^{d/2}$ of DJF seasons for the d-dimensional plot.

and then the maximum size of the dimension utilized is at most 3. However, most of significant variations in the tropospheric LFV dynamics would not be represented even in a three-dimensional phase space. The limitation could be avoided using a very-long-term integration of a GCM (Branstator and Berner 2005). If we want to represent ¾ of the tropospheric LFV variations, a 100 000-yr GCM integration should be conducted to create enough data to plot the PDF in a 10-dimensional phase space. It is also quite interesting to extend our study to examine the predictability of extratropical LFV occurring in a long-term GCM integration under the ''perfect model'' scenario. In this case, the predictability of the LFV of the GCM should be assessed by the spread of ensemble ''forecast'' conducted by the same GCM, and the empirical error growth should be evaluated in a phase space constructed by leading EOFs of the LFV in the GCM. The comparison between the ensemble spread and the empirical error growth obtained in the same GCM simulation would clarify the relevance of our new theory on the forecast error growth in exploring the predictability of the LFV since the result is totally free from the model bias. Moreover, our studies would be applied to a different geophysical fluid like the oceans, a different spatial domain like the stratosphere and the Southern Hemisphere, and different seasons. These extensive works will be left for our near-future studies.

Acknowledgments. The authors thank two anonymous reviewers, the MæT group in Hokkaido University, Prof. Masahide Kimoto, Prof. Takeshi Enomoto, and Prof. Shoshiro Minobe for giving us insightful comments for the study. This study was partly supported by Research Program on Climate Change Adaptation, by Grants-in-Aid for Scientific Research on Innovative Areas 22106008, by the Core Research for Evolution Science and Technology, and for Scientific Research (B) 23340141, all funded by the Ministry of Education, Culture, Sports, Science, and Technology of Japan. Prof. Takashi Sakajo in Hokkaido University especially supported our work. Figures were drawn using Grid Application Development Software.

REFERENCES

Berner, J., 2005: Linking nonlinearity and non-Gaussianity of planetary wave behavior by the Fokker–Planck equation. *J. Atmos. Sci.,* **62,** 2098–2117.

Branstator, G., and J. Berner, 2005: Linear and nonlinear signatures in the planetary wave dynamics of an AGCM: Phase space tendencies. *J. Atmos. Sci.,* **62,** 1792–1811.

Cehelsky, P., and K. K. Tung, 1987: Theories of multiple equilibria and weather regimes–A critical reexamination. Part II: Baroclinic two-layer models. *J. Atmos. Sci.,* **44,** 3282–3303.

Charney, J. G., and J. G. DeVore, 1979: Multiple flow equilibria in the atmosphere and blocking. *J. Atmos. Sci.,* **36,** 1205–1216.

Chikamoto, Y., H. Mukougawa, T. Kubota, A. Ito, and S. Maeda, 2007: Evidence of growing bred vector associated with the tropical intraseasonal oscillation. *Geophys. Res. Lett.,* **34,** L04806, doi:10.1029/2006GL028450.

Geisler, J. E., M. L. Blackmon, G. T. Bates, and S. Muñoz, 1985: Sensitivity of January climate response to the magnitude and position of equatorial Pacific sea surface temperature anomalies. *J. Atmos. Sci.,* **42,** 1037–1049.

Hasselmann, K., 1976: Stochastic climate models. Part I. Theory. *Tellus,* **28,** 473–484.

Horel, J. D., and J. M. Wallace, 1981: Planetary-scale atmospheric phenomena associated with the Southern Oscillation. *Mon. Wea. Rev.,* **109,** 813–829.

Itoh, H., 2008: Reconsideration of the true versus apparent Arctic Oscillation. *J. Climate,* **21,** 2047–2062.

——, and M. Kimoto, 1996: Multiple attractors and chaotic itinerancy in a quasigeostrophic model with realistic topography: Implications for weather regimes and low-frequency variability. *J. Atmos. Sci.,* **53,** 2217–2231.

Kalnay, E., 2003: *Atmospheric Modeling, Data Assimilation, and Predictability*. Cambridge University Press, 341 pp.

Kimoto, M., and M. Ghil, 1993: Multiple flow regimes in the Northern Hemisphere winter. Part I: Methodology and hemispheric regimes. *J. Atmos. Sci.,* **50,** 2625–2643.

——, H. Mukougawa, and S. Yoden, 1992: Medium-range forecast skill variation and blocking transition: A case study. *Mon. Wea. Rev.,* **120,** 1616–1627.

Legras, B., and M. Ghil, 1985: Persistent anomalies, blocking and variations in atmospheric predictability. *J. Atmos. Sci.,* **42,** 433–471.

Lorenz, E. N., 1965: A study of the predictability of a 28-variable atmospheric model. *Tellus,* **17,** 321–333.

Mo, K. T., and M. Ghil, 1988: Cluster analysis of multiple planetary flow regimes. *J. Geophys. Res.,* **93** (D9), 10 927–10 952.

Molteni, F., S. Tibaldi, and T. N. Palmer, 1990: Regimes in the wintertime circulation over Northern Extratropics. I: Observational evidence. *Quart. J. Roy. Meteor. Soc.,* **116,** 31–67.

Mukougawa, H., 1988: A dynamical model of quasi-stationary states in large-scale atmospheric motions. *J. Atmos. Sci.,* **45,** 2868–2888.

——, M. Kimoto, and S. Yoden, 1991: A relationship between local error growth and quasi-stationary states: Case study in the Lorenz system. *J. Atmos. Sci.,* **48,** 1231–1237.

——, T. Hirooka, and Y. Kuroda, 2009: Influence of stratospheric circulation on the predictability of the tropospheric Northern Annular Mode. *Geophys. Res. Lett.,* **36,** L08814, doi:10.1029/2008GL037127.

Newman, M., P. D. Sardeshmukh, C. R. Winkler, and J. S. Whitaker, 2003: A study of subseasonal predictability. *Mon. Wea. Rev.,* **131,** 1715–1732.

Onogi, K., and Coauthors, 2007: The JRA-25 Reanalysis. *J. Meteor. Soc. Japan,* **85,** 369–432.

Palmer, T. N., 1988: Medium and extended range predictability and stability of the PNA mode. *Quart. J. Roy. Meteor. Soc.,* **114,** 691–713.

——, 1999: A nonlinear dynamical perspective on climate prediction. *J. Climate,* **12,** 575–591.

Paul, W., and J. Baschnagel, 1999: *Stochastic Processes: From Physics to Finance.* Springer Verlag, 231 pp.

Penland, C., 2003: Noise out of chaos and why it won't go away. *Bull. Amer. Meteor. Soc.,* **84,** 921–925.

——, and L. Matrosova, 1998: Prediction of tropical Atlantic sea surface temperature using linear inverse modeling. *J. Climate,* **11,** 483–496.

Quadrelli, R., and J. M. Wallace, 2004: A simplified linear framework for interpreting patterns of Northern Hemisphere wintertime climate variability. *J. Climate,* **17,** 3728–3744.

Reinhold, B. B., and R. T. Pierrehumbert, 1982: Dynamics of weather regimes: Quasi-stationary waves and blocking. *Mon. Wea. Rev.,* **110,** 1105–1145.

Sura, P., M. Newman, C. Penland, and P. Sardeshmukh, 2005: Multiplicative noise and non-Gaussianity: A paradigm for atmospheric regimes? *J. Atmos. Sci.,* **62,** 1391–1409.

Tang, Y., H. Lin, J. Derome, and M. K. Tippett, 2007: A predictability measure applied to seasonal predictions of the Arctic Oscillation. *J. Climate,* **20,** 4733–4750.

Thompson, D. W. J., and J. M. Wallace, 2000: Annular modes in the extratropical circulation. Part I: Month-to-month variability. *J. Climate,* **13,** 1000–1016.

Wallace, J. M., and D. S. Gutzler, 1981: Teleconnections in the geopotential height field during the Northern Hemisphere winter. *Mon. Wea. Rev.,* **109,** 784–812.

Whitaker, J. S., and P. D. Sardeshmukh, 1998: A linear theory of extratropical synoptic eddy statistics. *J. Atmos. Sci.,* **55,** 237–258.

Yamane, S., and S. Yoden, 1997: Predictability variation and quasi-stationary states in simple non-linear systems. *J. Meteor. Soc. Japan,* **75,** 557–568.